mathematics

MDPI

Article

Motion of an Unbalanced Impact Body Colliding with a Moving Belt

Marek Lampart [1,2,*] **and Jaroslav Zapoměl** [3,4]

1 IT4Innovations, VSB—Technical University of Ostrava, 17. Listopadu 2172/15, 708 00 Ostrava, Czech Republic
2 Department of Applied Mathematics, VSB—Technical University of Ostrava, 17. Listopadu 2172/15, 708 00 Ostrava, Czech Republic
3 Department of Applied Mechanics, VSB—Technical University of Ostrava, 17. Listopadu 2172/15, 708 00 Ostrava, Czech Republic; jaroslav.zapomel@vsb.cz
4 Department of Dynamics and Vibrations, Czech Academy of Sciences, Institute of Thermomechanics, Dolejškova 1402/5, 182 00 Prague 8, Czech Republic
* Correspondence: marek.lampart@vsb.cz

Abstract: In the field of mechanical engineering, conveyors and moving belts are frequently used machine parts. In many working regimes, they are subjected to sudden loading, which can be a source of irregular motion in the impacting bodies and undesirable behavior in the working machine. This paper deals with a mechanical model where colisions between an impact body and a moving belt take place. The impact body is constrained by a flexible rope, the upper end of which is excited by a slider in the vertical direction. The behavior of the system was investigated in terms of its dependence on the amplitude and frequency of excitation given by the movement of the slider, and the eccentricity of the center of gravity of the impact body. Outputs of the computations indicate that different combinations of the analyzed parameters lead to high complexity of the system's movement. The bifurcation analysis shows multiple periodic areas changed by chaotic regions. The research carried out provides more details about the behavior and properties of strongly nonlinear mechanical systems resulting from impacts and dry friction. The obtained information will enable designers to propose parameters for industrial machines that make it possible to avoid their working at undesirable operating levels.

Keywords: mechanical model; impacts; 0–1 test for chaos; sample entropy; bifurcation

MSC: 37C60; 34H10; 34H20

check for updates

Citation: Lampart, M.; Zapoměl, J. Motion of an Unbalanced Impact Body Colliding with a Moving Belt. *Mathematics* **2021**, *9*, 1071. https://doi.org/10.3390/math9091071

Academic Editor: António M. Lopes

Received: 15 April 2021
Accepted: 6 May 2021
Published: 10 May 2021

Publisher's Note: MDPI stays neutral with regard to jurisdictional claims in published maps and institutional affiliations.

Copyright: © 2021 by the authors. Licensee MDPI, Basel, Switzerland. This article is an open access article distributed under the terms and conditions of the Creative Commons Attribution (CC BY) license (https://creativecommons.org/licenses/by/4.0/).

1. Introduction

Moving belts are machine parts that are frequently utilized in the area of mechanical engineering. They are applied for the transport of bodies or bulk materials and their processing. In many cases, the belts of conveyors operating in underground or surface mines, and crushing or milling plants, are subjected to impact loading caused by falling stones, blocks of rock, or crushing hammers. The impact forces, together with dry friction in the contact area, have a significant influence on the behavior of these devices, which is directly connected to the safety of the working process, adequate maintenance, and service life of the machinery. Because of this, conveyor belt machines have become a subject of analysis at many workplaces. Further technological motivations for the proposed research and applications can be found, e.g., in [1]; see also references therein.

Moon and Wickert [2] investigated the vibration of a power transmission belt system excited by pulleys exhibiting slight eccentricity through experiments and analytical methods. The experimentally observed jump and hysteresis phenomena in the near-resonant response were studied with a model that took into account nonlinear stretching of the

belt. Andreus and Casini [3] studied the movement of a body excited by a moving belt and colliding with a rigid and flexible obstacle. The varying nature of discontinuities arising in the combined problem of friction and impact was recognized and discussed. The authors presented closed-form solutions for both transient and steady-state responses, assuming Coulomb friction law and rigid stop-limiting motion. Chatterjee [4] presented a new approach to controlling friction-induced self-excited vibration (see also [5]). The investigated system consisted of a body flexibly connected to the frame and sliding on a moving belt. The control action was achieved by modulating the normal load at the frictional interface based on the state of the oscillatory system. These research results had a major impact on the theory of non-smooth dynamical systems that was developed in recent decades; see, e.g., [6,7]. This paper deals with searching for the control parameters.

This paper focuses on the impacts of an unbalanced impact body coupled with an elastic rope to a moving belt. The rope is set into motion at the upper end in the vertical direction. The impact body is unbalanced, which leads to eccentric collisions. Computational simulations were used to perform the research. The research outputs indicate that the character (regular or chaotic) of the system vibration induced by the impacts, dry friction, and motion of the belt depends on the frequency of the excitation, its amplitude, and the eccentricity of the impact body. This paper is a natural research continuation of the work with a much simpler model reported in [8], where the impact body was assumed to be balanced and results, contrary to this paper, were obtained for the parameters of two systems. In [9], a balanced case model is described with the assumption of a special case of an impact body that was taken as a cylinder.

The paper starts with the introduction, followed by the analyzed system (Section 2), and setting up of the mathematical model (Section 3). To achieve the aim of the paper, typical motion regimes are constructed (Section 4). Next, dynamics quantifiers and qualifiers are applied to the ranges of three parameters (Section 5) and, finally, bifurcations are observed (Section 6). Lastly, concluding remarks are made (Section 7).

2. The Analyzed System

The investigated system is presented in Figure 1 and it is composed of: a slider (1), impact body (2), flexible rope (3), conveyor belt (4), and rigid platform (5), see [8,9]. The slider performs a reciprocating sliding motion in the vertical direction. The impact body is of a complex shape consisting of a central cylinder and two end parts. The rope connects the slider with the center of the impact body. The belt moves in a horizontal direction at a constant velocity. The impact body performs a general planar motion. It can slide in the vertical and horizontal directions, and it can rotate about its axis. The rope transmits only the tensile force. All bodies of the system (except the rope) can be considered absolutely rigid. The flexibility of the rope makes it possible for the impact body to collide with the moving belt. Collisions can occur between the belt and the cylindrical part of the impact body. The material of the colliding bodies, in a small area near to the impact point and in a normal direction to the contact surfaces, is considered to be linearly elastic, exhibiting some material damping. As the impact body is unbalanced, the impacts are eccentric; the center of gravity of the impact body is marked T in Figure 1. The friction in the contact area is considered to be of a Coulomb type and the connection of the rope with the impact body and the slider is considered neutral (without resistances against the relative motion). The stiffness of the rope is linear, as is the damping of the impact body caused by the environment. From the point of view of time history, vertical motion of the slider is harmonic with a short transient period at the beginning.

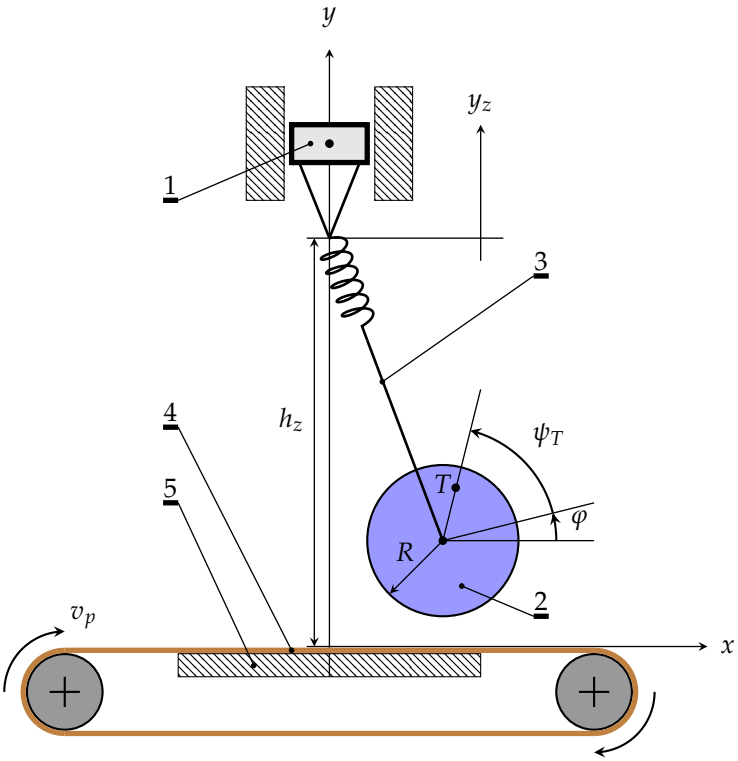

Figure 1. Scheme of the investigated system.

3. Mathematical Model of the System

The Lagrange equations of the second kind have been used to set up the motion equations:

$$\begin{array}{rcl} m\ddot{x} - me_T\ddot{\varphi}\sin(\varphi+\psi_T) - me_T\dot{\varphi}^2\cos(\varphi+\psi_T) & = & Q_x, \\ m\ddot{y} + me_T\ddot{\varphi}\cos(\varphi+\psi_T) - me_T\dot{\varphi}^2\sin(\varphi+\psi_T) & = & Q_y, \\ -me_T\ddot{x}\sin(\varphi+\psi_T) + me_T\ddot{y}\cos(\varphi+\psi_T) + (J_T+me_T^2)\ddot{\varphi} & = & Q_\varphi \end{array} \quad (1)$$

where

$$Q_x = F_x + F_t - b\dot{x}, \quad (2)$$

$$Q_y = F_y + F_c - mg - b\dot{y}, \quad (3)$$

$$Q_\varphi = F_t R - mge_T\cos(\varphi+\psi_T) - b_\varphi\dot{\varphi} \quad (4)$$

and x and y denote the position of the impact body center, and φ its angular rotation, see [8,9]. F_x, F_y, F_t, and F_c are x and y components of the forces, by which the suspension acts on the impact body; the tangential component of the contact force (friction force), and the normal component of the contact force acting on the impact body, respectively. $(\dot{})$ and $(\ddot{})$ stand for the first and second derivative with respect to time. The notations of the other quantities and their descriptions are shown in Table 1.

Extension of the impact body suspension Δl and its rate can be expressed as follows:

$$\Delta l = \sqrt{x^2 + (y - y_z - h_z)^2} - L_0,$$

$$\Delta\dot{l} = 1/2\left(x^2 + (y - y_z - h_z)^2\right)^{-1/2}(2x\dot{x} + 2(y - y_z - h_z)(\dot{y} - \dot{y}_z)).$$

Stiffness and material damping of the rope are considered to be linear. In addition, the rope transmits only the tensile force. This is expressed by

$$\begin{aligned} F_l = k_l \Delta l + b_l \Delta \dot{l} \quad & \text{for} \quad \Delta l > 0 \text{ and } k_l \Delta l + b_l \Delta \dot{l} > 0, \\ F_l = 0 \quad & \text{for} \quad \Delta l \leq 0 \text{ or } k_l \Delta l + b_l \Delta \dot{l} \leq 0. \end{aligned}$$

Then, for the horizontal axial force components acting on the impact body, it holds:

$$\begin{aligned} F_x &= -F_l \cos(\beta), \\ F_y &= -F_l \sin(\beta) \end{aligned} \tag{5}$$

where β follows from the solution of the following equations; see Figure 2:

$$\cos(\beta) = \frac{x}{\sqrt{x^2 + (y - y_z - h_z)^2}},$$

$$\sin(\beta) = \frac{y - y_z - h_z}{\sqrt{x^2 + (y - y_z - h_z)^2}}.$$

Table 1. Parameters of the system (1).

Quantity	Value	Description
m	10 kg	mass of the impact body
J_T	0.2 kg m^2	moment of inertia of the impact body referred to its center of gravity
ψ_T	0.4 rad	angular phase shift of the center of gravity
L_0	0.35 m	length of the unloaded suspension of the impact body
h_z	0.89 m	the mean hight of the excitation body above the belt
R	0.04 m	radius of the impact body
k_c	1×10^7 Nm^{-1}	contact stiffness (impact body–belt)
b_c	100 Nsm^{-1}	the coefficient of contact damping (impact body–belt)
k_l	200 N m^{-1}	stiffness of the impact body suspension
b_l	5 Nsm^{-1}	the damping coefficient of the impact body suspension
g	9.80665 m s^{-2}	the gravity acceleration
α	1 s^{-1}	the run up coefficient
v_p	0.5 ms^{-1}	velocity of the belt
b	0.01 Ns m^{-1}	the outer damping coefficient of the impact body (sliding motion)
b_φ	0.001 Nms rad^{-1}	the outer damping coefficient of the impact body (rotational motion)
f	0.2	coefficient of friction
a	100 s m^{-1}	mathematical constant defining the shape of the friction characteristic

The contact stiffness and damping are considered to be linear and the contact force can be only compressive. Then, for each magnitude, it holds that

$$F_c = k_c(R - y) - b_c \dot{y} \quad \text{for} \quad y < R \text{ and } k_c(R - y) - b_c \dot{y} > 0, \tag{6}$$

$$F_c = 0 \quad \text{for} \quad y \geq R \text{ or } k_c(R - y) - b_c \dot{y} \leq 0. \tag{7}$$

For the friction force acting on the impact body, it holds that

$$F_t = -\frac{2F_c f}{\pi} \text{atan}(a(\dot{x} + R\dot{\varphi} - v_p)). \tag{8}$$

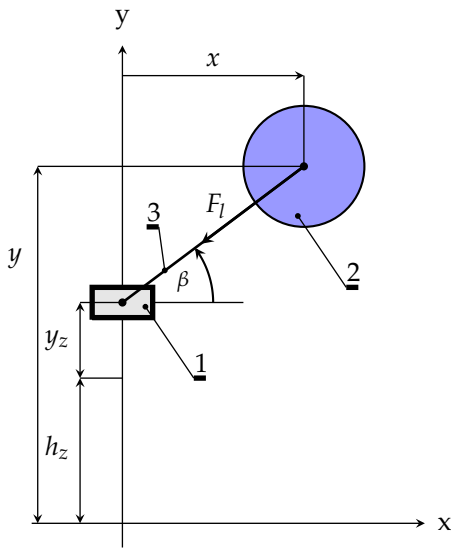

Figure 2. Decomposition of the force F_l.

The vertical position of the driving body is given by

$$y_z(t) = z_a(1 - e^{-\alpha t})\sin(\omega t) \tag{9}$$

where z_a is the amplitude of the driving body kinetic excitation, α is the run up coefficient, and ω stands for the excitation frequency. The time history of the position of the sliding body is y_z, which excites the system as shown in Figure 3.

At the beginning, the system takes the rest position defined by the following initial conditions:

$$\begin{array}{ll} x(0) = 0, & \dot{x}(0) = 0, \\ y(0) = h_z - L_0 - mg/k_l, & \dot{y}(0) = 0, \\ \varphi(0) = -\pi/2 - \psi_T, & \dot{\varphi}(0) = 0. \end{array}$$

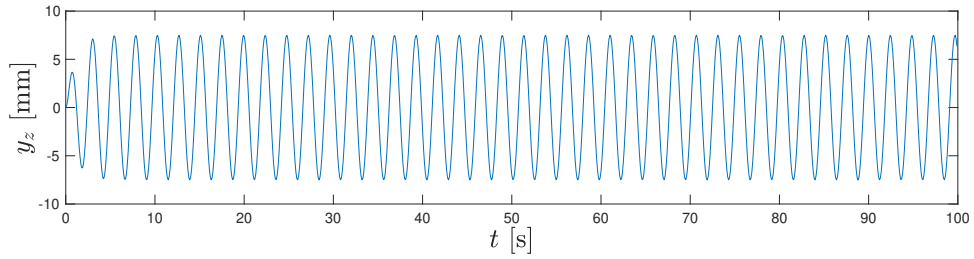

Figure 3. The function y_z (9) for $\omega = 2.6$ rad s^{-1}, $z_a = 7.5$ mm, and the parameters set in Table 1.

4. Periodic, Quasi-Periodic, Chaotic Motion

The examinated system (1) is described by 20 parameters, 17 of which (given in Table 1) are fixed for all further simulations. The last three, the excitation frequency ω, amplitude z_a, and eccentricity e_T, will be variable, illustrating the richness of dynamics that the model accounts for.

Firstly, three study cases are given: periodic, quasi-periodic, and chaotic. In all cases, there are given time histories, phase portraits with the Fourier spectra, and corresponding forces. The contact force F_c given by ((6) and (7)), the friction force F_t derived in (8), and the elastic force in the rope

$$F_r = \sqrt{F_x^2 + F_y^2} \tag{10}$$

underline the movement character of entire bodies.

For if $e_T = 0.015$ m, ω =4 rad s^{-1}, and $z_a = 0.009$ m, the movement is periodic, as shown in Figures 4–6. In this case, the time histories (Figure 4) generate a T1 periodic loop

in the phase portrait (Figure 5—left), with detectable contact between the impact body and belt. The corresponding FFT (Figure 5—right) shows single frequencies that correspond to periodicity. The forces (Figure 6) are given for completeness.

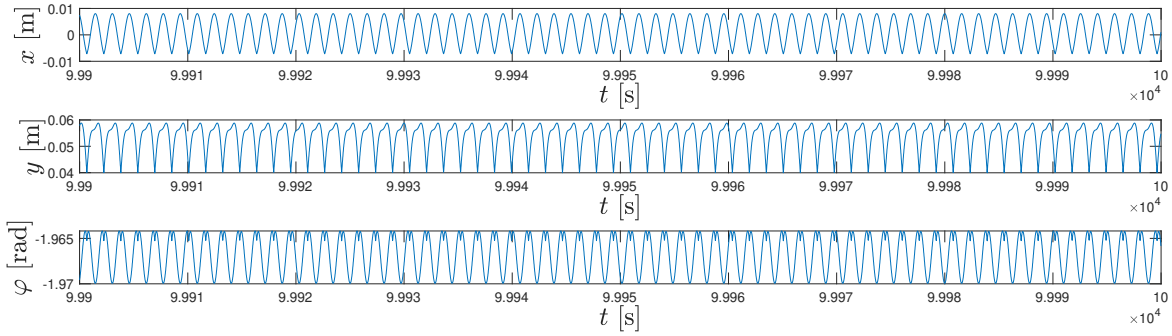

Figure 4. Investigated system's (1) time histories of x, y, and φ for $e_T = 0.015$ m, ω =4 rad s^{-1}, and $z_a = 0.009$ m.

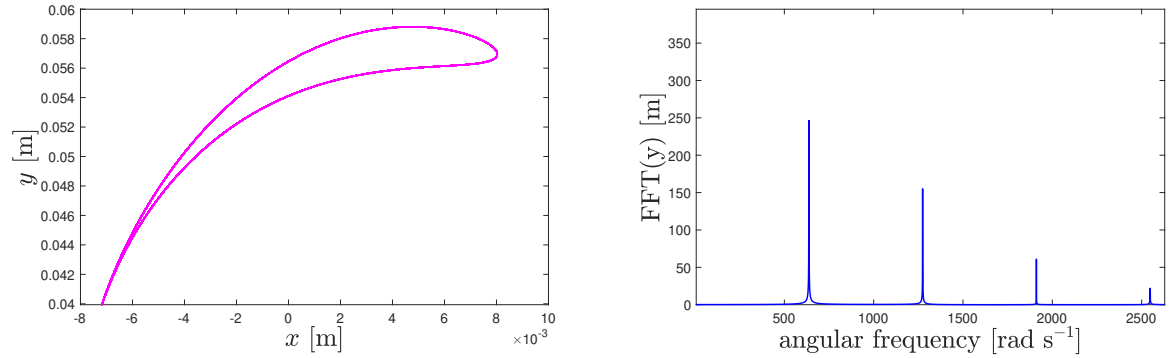

Figure 5. Investigated system's (1) phase diagram and FFT(y) for $e_T = 0.015$ m, ω =4 rad s^{-1}, and $z_a = 0.009$ m.

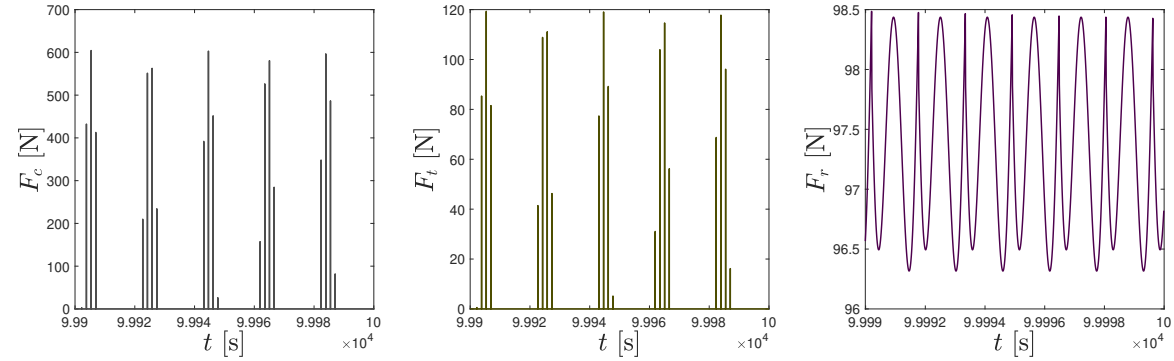

Figure 6. Investigated system's (1) forces F_c, F_t, and F_r for $e_T = 0.015$ m, ω =4 rad s^{-1}, and $z_a = 0.009$ m.

Next, let $e_T = 0.02$ m, ω =2.8 rad s^{-1}, and $z_a = 0.0056$ m; then, the movement is quasi-periodic, as shown in Figures 7–9. The time histories (Figure 7) used for the construction of the phase portrait (Figure 8—left) behave in a quasi-periodic mode; contacts between the impact body and belt are detectable. The corresponding FFT (Figure 8—right) confirms the quasi-periodic trajectory, since, on every main frequency, only few-sided frequencies appear. The forces (Figure 9) are given for completeness.

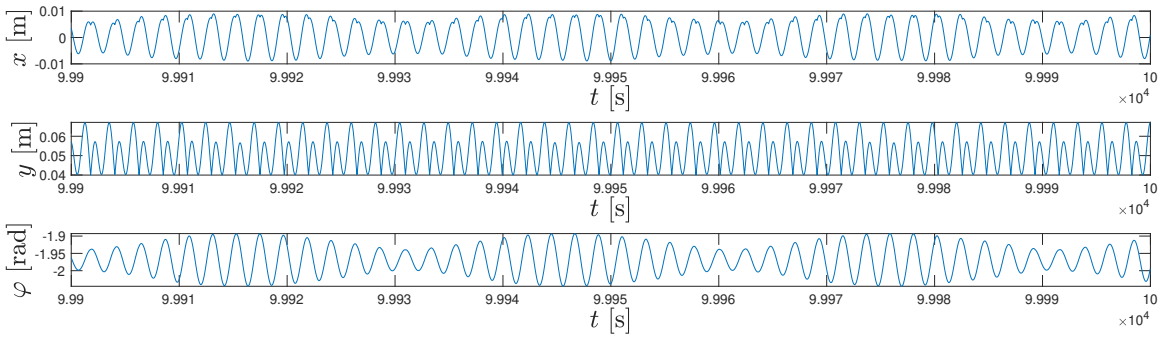

Figure 7. nvestigated system's (1) time histories of x, y, and φ for $e_T = 0.02$ m, ω =2.8 rad s^{-1}, and $z_a = 0.0056$ m.

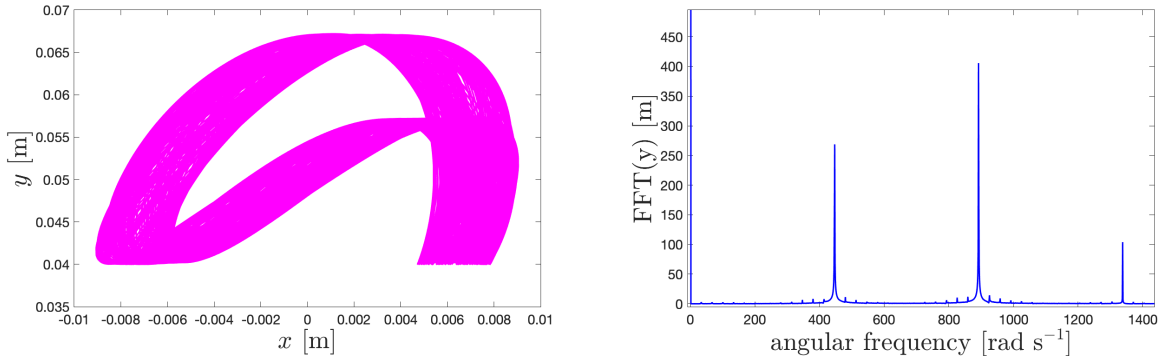

Figure 8. Investigated system's (1) phase diagram and FFT(y) for $e_T = 0.02$ m, ω =2.8 rad s^{-1}, and $z_a = 0.0056$ m.

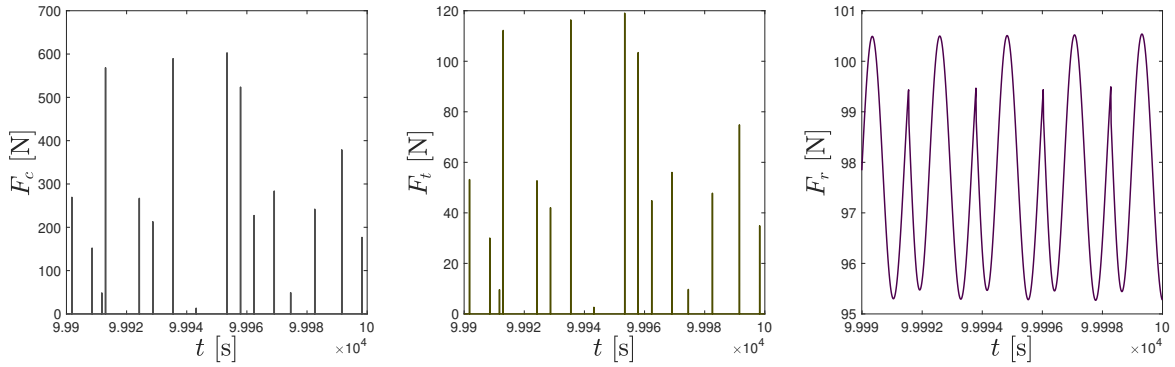

Figure 9. Investigated system's (1) forces F_c, F_t, and F_r for $e_T = 0.02$ m, ω =2.8 rad s^{-1}, and $z_a = 0.0056$ m.

Finally, if parameters are set as $e_T = 0.015$ m, ω =2.2 rad s^{-1}, and $z_a = 0.0028$ m, then the movement is chaotic, as is visible in Figures 10–12. In this case, the time histories (Figure 10) together with the phase portrait (Figure 11—left) detect contacts between the impact body and the belt. The corresponding FFT (Figure 11—right) validates chaos, since, on every main frequency, there are superposed wide bands of both-sided frequencies. The forces (Figure 12) are given for completeness.

Hence, it can be concluded that:

Property 1. *There are system (1) parameters e_T, ω, and z_a such that its movement character is:*

1. *periodic (for, e.g., $e_T = 0.015$ m, ω =4 rad s^{-1}, and $z_a = 0.009$ m),*
2. *quasi-periodic (for, e.g., $e_T = 0.02$ m, ω =2.8 rad s^{-1}, and $z_a = 0.0056$ m), and*
3. *chaotic (for, e.g., $e_T = 0.015$ m, ω =2.2 rad s^{-1}, and $z_a = 0.0028$ m).*

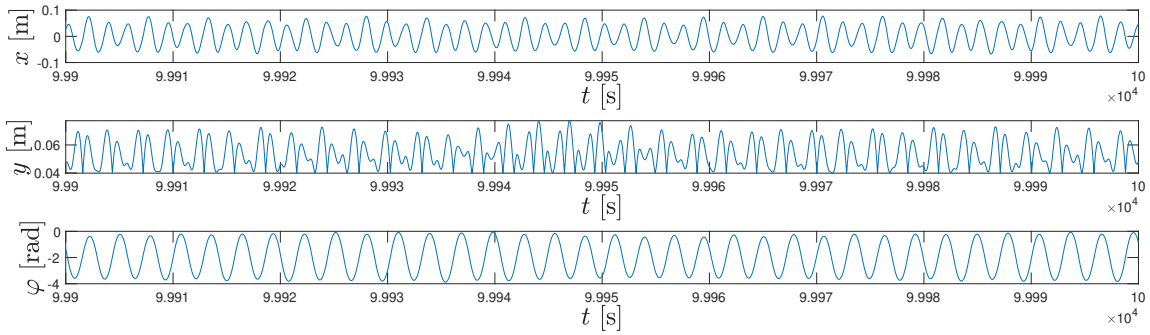

Figure 10. Investigatedsystem's (1) time histories of x, y, and φ for $e_T = 0.015$ m, ω =2.2 rad s^{-1}, and $z_a = 0.0028$ m.

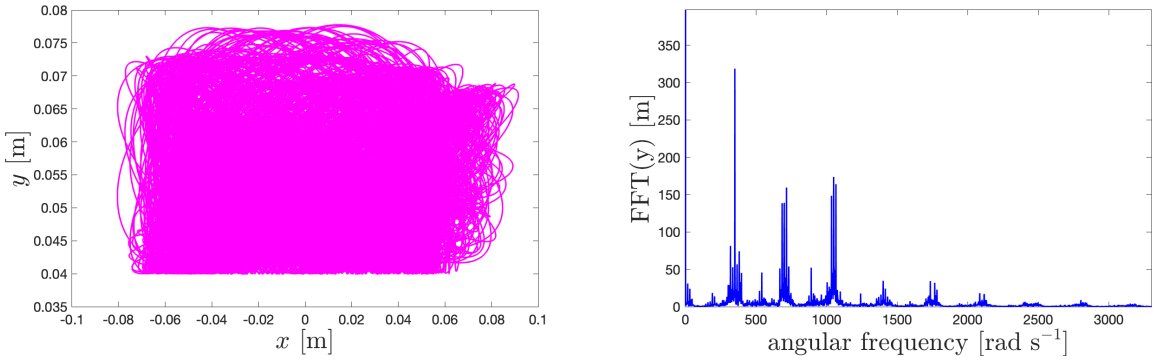

Figure 11. Investigated system's (1) phase diagram and FFT(y) for $e_T = 0.015$ m, ω =2.2 rad s^{-1}, and $z_a = 0.0028$ m.

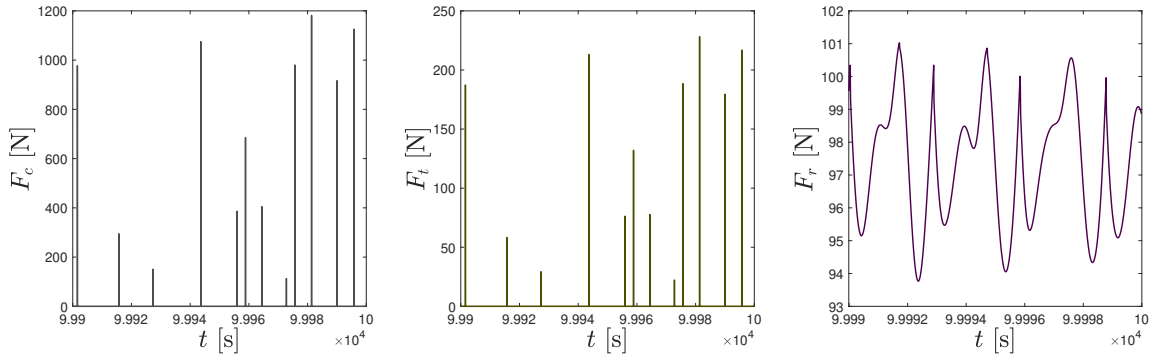

Figure 12. Investigated system's (1) forces F_c, F_t, and F_r for $e_T = 0.015$ m, ω =2.2 rad s^{-1}, and $z_a = 0.0028$ m.

The proof of Property 2 is given by computer graphics analysis studying the phase diagrams together with FFT (Figures 5, 8, and 11—left) underlined by their time histories in Figures 4, 7, and 10. This dynamic behavior coincides with K and E_{Samp} shown in Figures 13–15 parts (b,c). It is also worth remarking that the same movement's patterns are visible on related forces in Figures 6, 9, and 12.

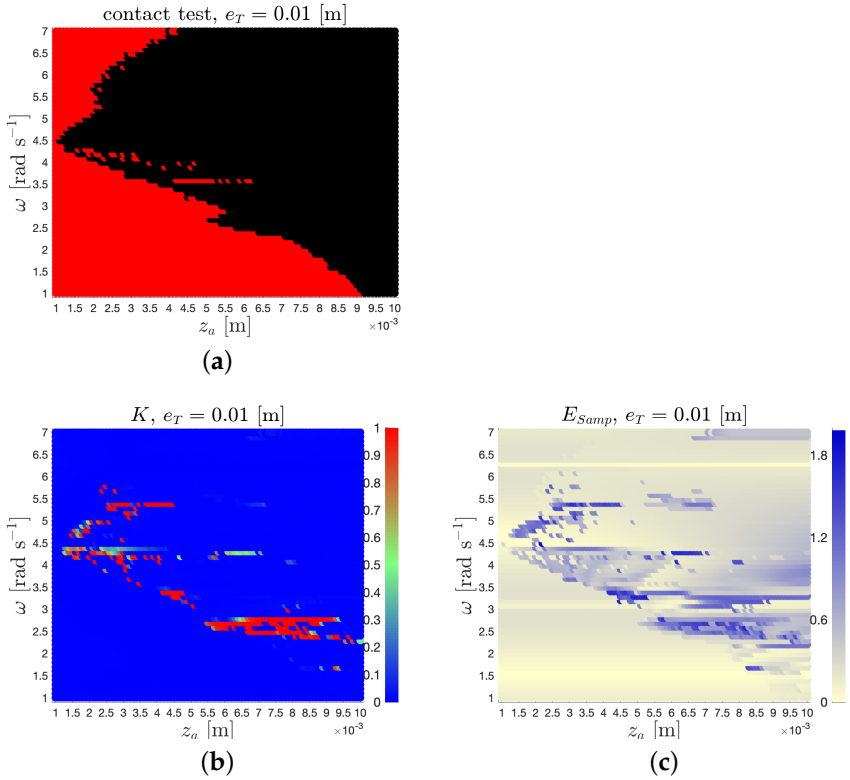

Figure 13. Outputs of the contact test (**a**), the 0–1 test for chaos K (**b**), and sample entropy E_{Samp} (**c**) for eccentricity e_T of 0.01 m with respect to the excitation frequency ω and amplitude z_a.

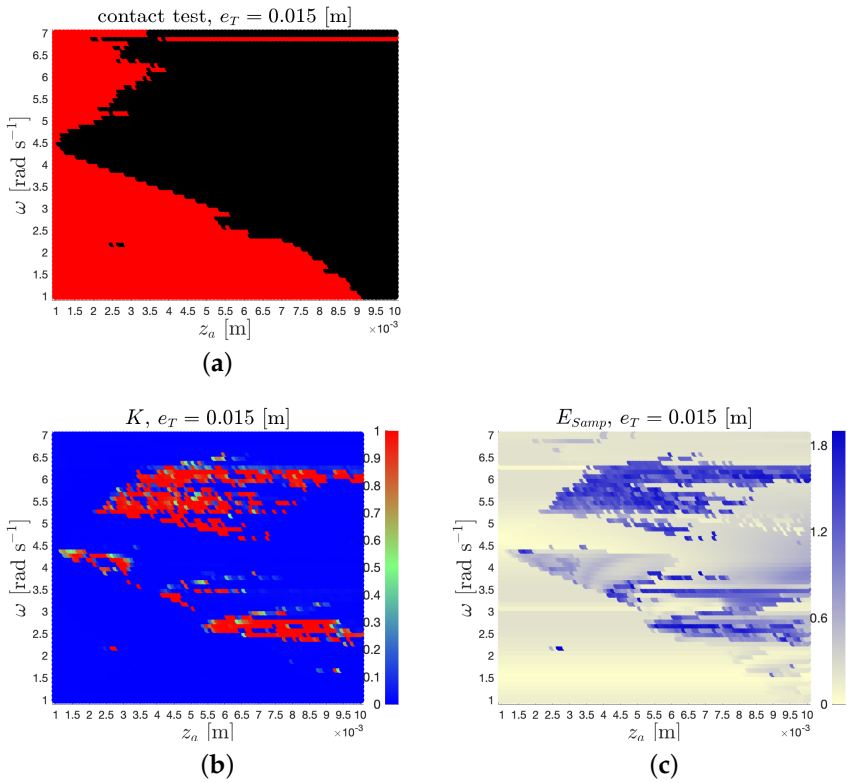

Figure 14. Outputs of the contact test (**a**), the 0–1 test for chaos K (**b**), and sample entropy E_{Samp} (**c**) for eccentricity e_T of 0.015 m with respect to the excitation frequency ω and amplitude z_a.

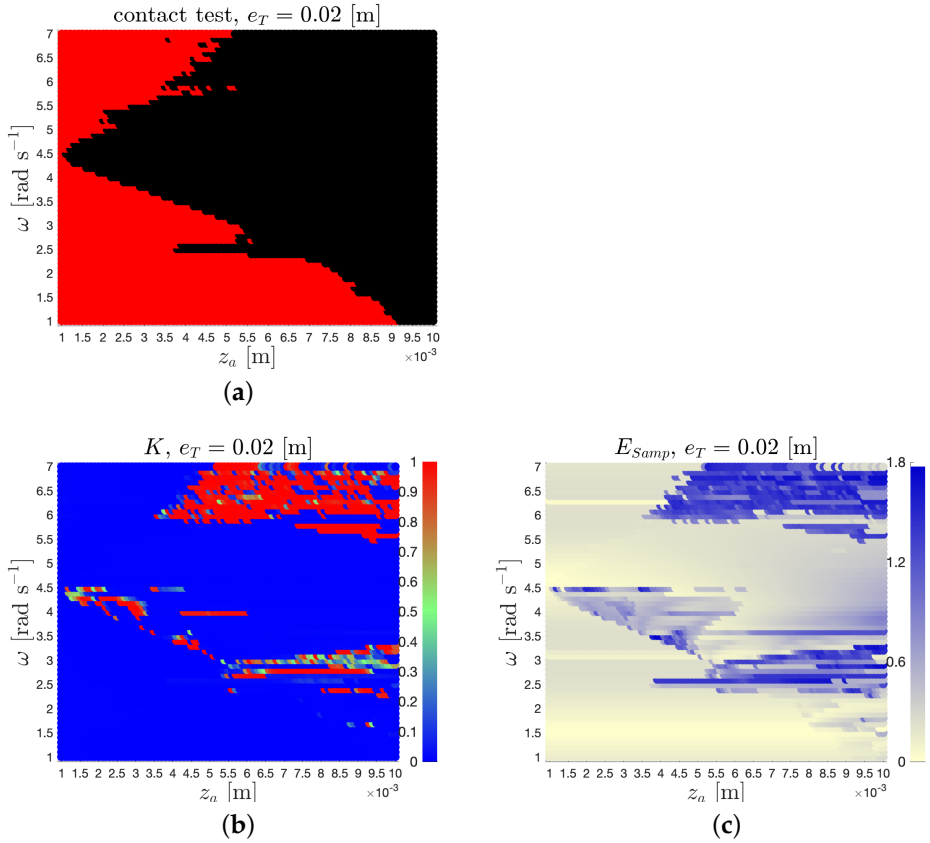

Figure 15. Outputs of the contact test (**a**), the 0–1 test for chaos K (**b**), and sample entropy E_{Samp} (**c**) for eccentricity e_T of 0.02 m with respect to the excitation frequency ω and amplitude z_a.

Consequently, it can be concluded that:

Property 2. *Let $e_T \in \{0.01, 0.015, 0.02\}$. If the system's (1) trajectory is chaotic, then the impact body (body 2, Figure 1) comes into contact with the belt (body 4, Figure 1).*

5. Three Parameters' Dynamics Depiction

In the previous section, for characterization of the movement, the combination of phase portraits with FFT was used. This method is applicable only in single cases. Hence, for further investigation, a combination of newly established tests is used. These are the 0–1 test for chaos (K for brevity) and sample entropy (denoted E_{Samp}).

The dynamics quantifier K was introduced by [10] (see also [11]) and gives binary outputs. If K is close to zero (denoted by blue in our results), regular movements appear, and when K approaches one, there is chaos (marked in red). It is possible to apply this test to the full variety of the time series corresponding to the real data [12] and time series derived by continuous [13,14] or discrete models [15].

As a dynamical quantifier, E_{Samp} is utilized. This tool was introduced by [16] and used in wide range of research areas [17–19]. As an output, E_{Samp} gives a value that measures the complexity of the system; as E_{Samp} increases, the complexity increases.

The evaluation of the movement character was performed in the free software environment R [20] using the packages *Chaos01* [21] and *TSEntropies* [22]. This dynamics mining process was applied on simulation outputs that were obtained by the Runge–Kutta method of the fourth order using MATLAB [23] (solver *ode45*). Each simulation was performed on 10^5 s with recorded 10^7 values. To eliminate the distortions of the system, only the last 20% of simulated data were examined. The imput vector ϕ of the K and E_{Samp} tests is assembled as the Euclidean norm of state variables x and y:

$$\phi(j) = \sqrt{x(j)^2 + y(j)^2}.$$

As mentioned above, there were three driving parameters detected, for which the following simulations were performed:

$$e_T \times z_a \times \omega = \{0.01,\ 0.015,\ 0.02\} \times [0.001, 0.01] \times [1, 7].$$

Individual cases of $e_T \in \{0.01,\ 0.015,\ 0.02\}$ are shown in Figures 13–15. There are given dynamics characteristics K and E_{Samp} together with the output of the contact test of the impact body with the belt. It is worthy to note, that the results of K and E_{Samp} coincide and the complexity (or number of chaotic cases) increases while e_T increases (see Figures 13–15 parts (b,c)). The area of $z_a \times \omega$ parameters for which contacts appears is slightly variable in respect to e_T. Moreover, it is observable that small contacts regions are surrounded by non-contact cases and vice versa (compare Figures 13 and 15 parts (a); in these figures, contact cases are marked in black and non-contact by red).

The proof of Property 2 is given by computer graphics analysis studying the 0–1 test for chaos K and sample entropy E_{Samp} comparing to their corresponding contact tests, which is given in Figures 13–15. Note that the inverse implication of Property 2 is not valid. As a counter-example, the system's (1) parameters can be as those related in Figures 4–6.

6. Bifurcation Analysis

To show the genesis of the high complexity movement from the low one, and vice versa, the bifurcation analysis on a restriction of $z_a \times \omega$ is given for $z_a = 0.008$ m supported by K and E_{Samp} characteristics. For this purpose, bifurcation diagrams depending on $\omega \in [2, 7]$ rad s^{-1}, and its magnification for $\omega \in [2, 3]$ rad s^{-1}, are constructed. The bifurcation diagrams (Figures 16 and 17) were constructed using the projection technique of local maxima (dark gray) together with local minima (light gray); the maximum (green line) and minimum (red line) values are also given for completeness. Figure 16 corresponds to the x variable and Figure 17 to y, while the parts indexed with "2" (right column figures) show a magnification of relevant "1" indexes (left column figures). These bifurcation diagrams show an increase in complexity when e_T increases. It is also observable that there are numerous periodic windows, with a period doubling effect, surrounded by chaotic cases.

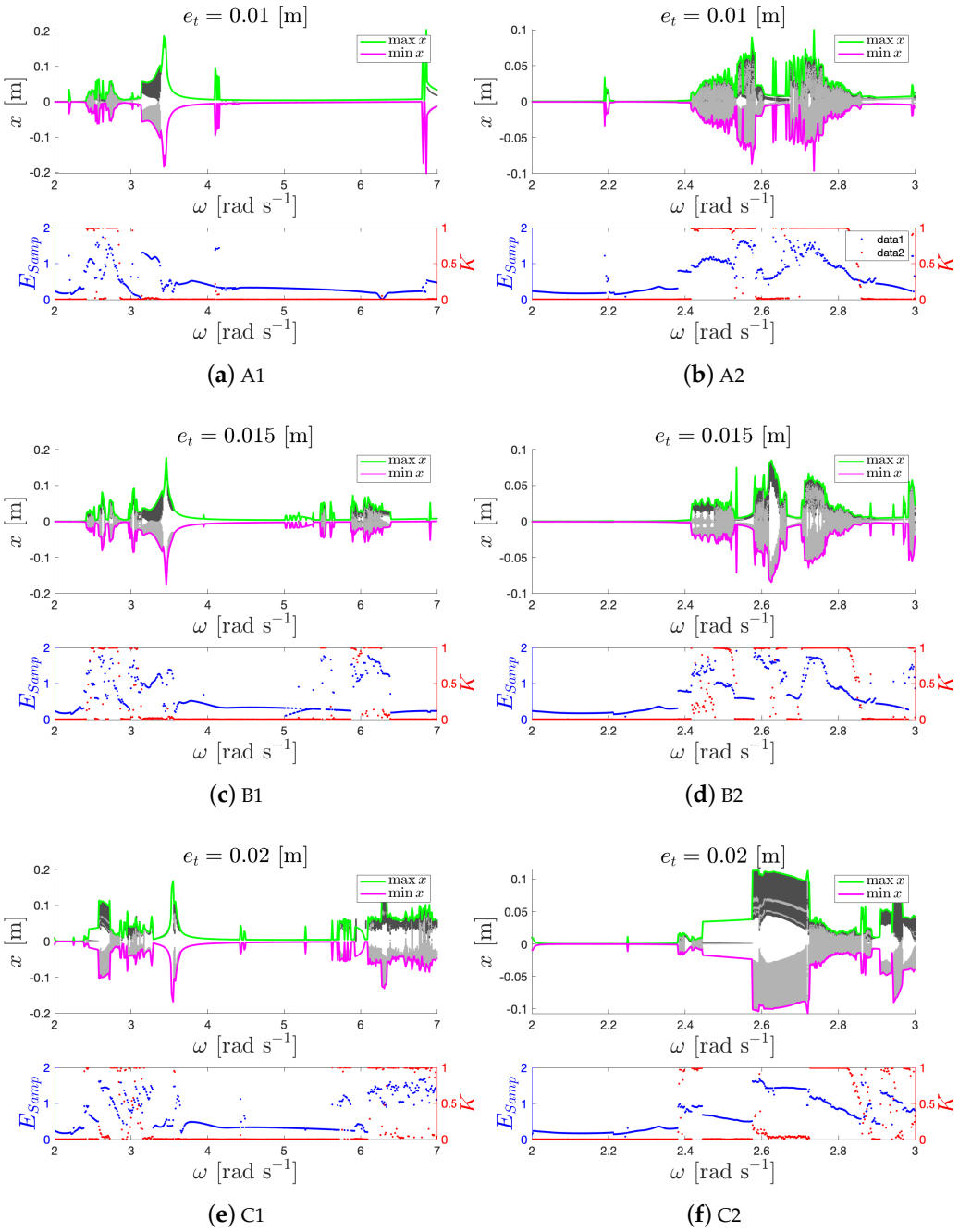

(a) A1 **(b)** A2

(c) B1 **(d)** B2

(e) C1 **(f)** C2

Figure 16. Bifurcation diagrams and outputs of the 0–1 test for chaos K and sample entropy E_{Samp} of x for $z_a = 0.008$ m with respect to the excitation frequency ω rad s^{-1} of the sliding body: the first-column cases correspond to $\omega \in [2,7]$ rad s^{-1} while the second-column cases to their magnifications $\omega \in [2,3]$ rad s^{-1}, and "A", "B", "C" to eccentricity e_T of 0.01 m, 0.015 m, and 0.02 m, respectively.

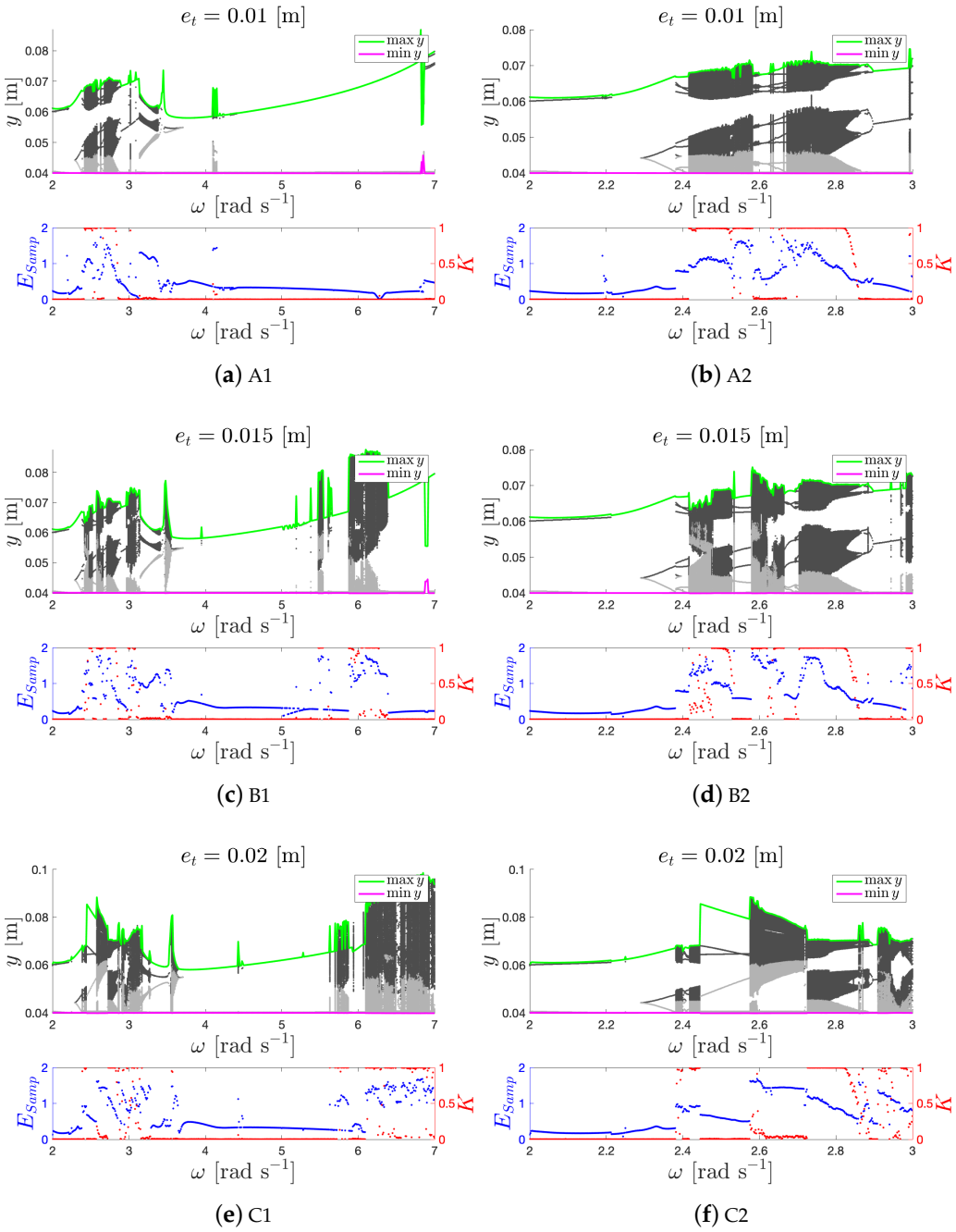

(a) A1 **(b)** A2

(c) B1 **(d)** B2

(e) C1 **(f)** C2

Figure 17. Bifurcation diagrams and outputs of the 0–1 test for chaos K and sample entropy E_{Samp} of y for $z_a = 0.008$ m with respect to the excitation frequency ω rad s^{-1} of the sliding body: the first-column cases correspond to $\omega \in [2,7]$ rad s^{-1} while the second-column cases to their magnifications $\omega \in [2,3]$ rad s^{-1}, and "A", "B", "C" to eccentricity e_T of 0.01 m, 0.015 m, and 0.02 m, respectively.

7. Conclusions

In this paper, a newly constructed mechanical system consisting of an unbalanced impact body constrained by a flexible rope and a moving belt is derived. This model was researched under massive numerical simulation, and its impressive dynamics were revealed.

To accomplish this, a model of three degrees of freedom was built and then simulated in MATLAB [23] using the Runge–Kutta method as an in-function *ode45* adaptive solver, and a final evaluation was performed in R [20] applying the *Chaos01* [21] and *TSEntropies* [22] packages.

The primary results show that all possible types of movement character can be stimulated (Property 1); period, quasi-period, and chaos (Figures 5, 8, and 11). For the completeness of the study, all forces are also given: F_c, F_t, and F_r (Figures 6, 9, and 12).

Next, the dynamics qualifier K and quantifier E_{Samp} were applied to a range of three parameters: $e_T \times z_a \times \omega$; Figures 13–15. The necessary condition for chaotic movement (contact) was observed (Property 2). It is also noteworthy that the statistical success of the 0–1 test for chaos was over 96% (see Table 2). Here, successful outputs of K are marked (in blue for regularity and red for chaos) if their value is in the interval $(0, 0.1)$ for regular cases and $(0.9, 1)$ for chaotic ones.

Finally, bifurcation analysis was performed, showing multiple periodic windows followed by chaotic bands (Figures 16 and 17).

Table 2. Statistical success of the 0–1 test for chaos.

e_T [m]	# Reg. Cases	# Chaotic Cases	# Decidable Cases	Test Success
0.01	5293	162	5455	98.27%
0.015	4808	542	5350	96.38%
0.02	4740	593	5333	96.07%

Author Contributions: The authors contributed to the paper equally. All authors have read and agreed to the published version of the manuscript.

Funding: This research received no external funding.

Institutional Review Board Statement: Not applicable.

Informed Consent Statement: Not applicable.

Data Availability Statement: Not applicable.

Acknowledgments: This work was supported by The Ministry of Education, Youth and Sports from the National Programme of Sustainability (NPU II) project "IT4Innovations excellence in science—LQ1602"; by The Ministry of Education, Youth and Sports from the Large Infrastructures for Research, Experimental Development, and Innovations project "e-INFRA CZ—LM2018140"; by Grant of SGS No. SP2021/103, VŠB—Technical University of Ostrava, Czech Republic; and by grant project of the Czech Science Foundation 19-06666S.

Conflicts of Interest: The authors declare no conflict of interest.

References

1. Lancioni, G.; Lenci, S.; Galvanetto, U. Non-linear dynamics of a mechanical system with a frictional unilateral constraint. *Int. J. Non-Linear Mech.* **2009**, *44*, 658–674. [CrossRef]
2. Moon, J.; Wickert, J.A. Non-linear vibration of power transmission belts. *J. Sound Vib.* **1997**, *200*, 419–431. [CrossRef]
3. Andreaus, U.; Casini, P. Friction oscillator excited by moving base and colliding with a rigid or deformable obstacle. *Int. J. Non-Linear Mech.* **2002**, *37*, 117–133. [CrossRef]
4. Chatterjee, S. Non-linear control of friction-induced self-excited vibration. *Int. J. Non-Linear Mech.* **2007**, *42*, 459–469. [CrossRef]
5. Lampart, M.; Zapoměl, J. Vibrations attenuation of a system excited by unbalance and the ground movement by an impact element. *Appl. Math. Nonlinear Sci.* **2016**, *1*, 603–616. [CrossRef]
6. Di Bernardo, M.; Budd, C.J.; Champneys, A.R.; Kowalczyk, P. *Piecewise-Smooth Dynamical Systems Theory and Applications*; Applied Mathematical Sciences (Switzerland); Springer: London, UK, 2008; Volume 163, pp. 1–481.
7. Awrejcewicz, J.; Lamarque, C.H. *Bifurcation and Chaos in Nonsmooth Mechanical Systems*; World Scientific Series on Nonlinear Science Series A: Volume 45; World Scientific: Singapore, 2003; p. 564.
8. Lampart, M.; Zapoměl, J. Chaos identification of a colliding constrained body on a moving belt. *Nonlinear Dyn.* **2021**. [CrossRef]
9. Lampart, M.; Zapoměl, J. On regular and irregular movement of cylinder colliding with a moving belt. *J. Phys. Conf. Ser.* **2021**, *1730*, 012093. [CrossRef]
10. Gottwald, G.; Melbourne, I. A new test for chaos in deterministic systems. *Proc. R. Soc. Lond. A* **2004**, *460*, 603–611. [CrossRef]
11. Gottwald, G.; Melbourne, I. On the implementation of the 0–1 test for chaos. *SIAM J. Appl. Dyn. Syst.* **2009**, *8*, 129–145. [CrossRef]
12. Falconer, I.; Gottwald, G.A.; Melbourne, I.; Wormnes, K. Application of the 0–1 test for chaos to experimental data. *SIAM J. Appl. Dyn. Syst.* **2007**, *6*, 395–402. [CrossRef]

13. Lampart, M.; Zapoměl, J. The motion characteristics of the double-pendulum system with skew walls. *Math. Methods Appl. Sci.* **2019**, *42*, 475–487. [CrossRef]
14. Lampart, M.; Zapoměl, J. Dynamics of a non-autonomous double pendulum model forced by biharmonic excitation with soft stops. *Nonlinear Dyn.* **2020**, *99*, 1909–1921. [CrossRef]
15. Lampart, M.; Martinovič, T. Chaotic behavior of the CML model with respect to the state and coupling parameters. *J. Math. Chem.* **2019**, *57*, 1670–1681. [CrossRef]
16. Richman, J.S.; Moorman, J.R. Physiological time-series analysis using approximate and sample entropy. *Am. J. Physiol. Heart Circ. Physiol.* **2000**, *278*, H2039–H2049. [CrossRef]
17. Montesinos, L.; Castaldo, R.; Pecchia, L. On the use of approximate entropy and sample entropy with centre of pressure time-series. *J. Neuroeng. Rehabil.* **2018**, *15*, 116. [CrossRef]
18. Xiao, D.; Wang, J. Dynamic complexity and causality of crude oil and major stock markets. *Energy* **2020**, *193*, 116791. [CrossRef]
19. Li, S.; Zhou, Q.; Wu, S.; Dai, E. Measurement of climate complexity using sample entropy. *Int. J. Climatol.* **2006**, *26*, 2131–2139.
20. Team, R.C. *R: A Language and Environment for Statistical Computing*; R Foundation for Statistical Computing: Vienna, Austria, 2018.
21. Martinovič, T. *Chaos01: 0–1 Test for Chaos*; R Package Version 1.1.1; 2016. Available online: https://CRAN.R-project.org/package=Chaos01 (accessed on 12 April 2021).
22. Tomčala, J. *TSEntropies: Time Series Entropies*; R Package Version 0.9; 2018. Available online: https://CRAN.R-project.org/package=TSEntropies (accessed on 12 April 2021).
23. *MATLAB*; The MathWorks, Inc.: Natick, MA, USA, 2016.